Earth and Space Science

DATA ARTICLE
10.1029/2025EA004690

Key Points:

- Geophysical retrieval methods from the Advanced Microwave Precipitation Radiometer have been tested and validated in the maritime tropics
- Uncertainties in cloud liquid water path, total precipitable water vapor, and 10-m wind speed retrievals all fall within expected ranges
- The retrieval methods have science applications throughout a broader range of microwave radiometers and climatological regions

Supporting Information:

Supporting Information may be found in the online version of this article.

Correspondence to:
C. G. Amiot,
corey.amiot@uah.edu

Citation:
Amiot, C. G., Lang, T. J., van Diedenhoven, B., van den Heever, S. C., Carey, L. D., Freeman, S. W., & Sokolowsky, G. A. (2026). Airborne passive Microwave retrievals of Cloud liquid water, total precipitable water, and near-surface wind speed in the maritime tropics. *Earth and Space Science*, *13*, e2025EA004690. https://doi.org/10.1029/2025EA004690

Received 5 AUG 2025
Accepted 16 JAN 2026

Author Contributions:

Conceptualization: Corey G. Amiot, Timothy J. Lang, Bastiaan van Diedenhoven, Lawrence D. Carey
Data curation: Corey G. Amiot, Timothy J. Lang, Bastiaan van Diedenhoven, Susan C. van den Heever, Sean W. Freeman, G. Alexander Sokolowsky
Formal analysis: Corey G. Amiot
Funding acquisition: Timothy J. Lang
Investigation: Corey G. Amiot

Airborne Passive Microwave Retrievals of Cloud Liquid Water, Total Precipitable Water, and Near-Surface Wind Speed in the Maritime Tropics

Corey G. Amiot[1,2], Timothy J. Lang[3], Bastiaan van Diedenhoven[4], Susan C. van den Heever[5], Lawrence D. Carey[1], Sean W. Freeman[5,6], and G. Alexander Sokolowsky[5]

[1]Department of Atmospheric and Earth Science, The University of Alabama in Huntsville, Huntsville, AL, USA, [2]Now at Earth System Science Center, The University of Alabama in Huntsville, Huntsville, AL, USA, [3]NASA Marshall Space Flight Center, Huntsville, AL, USA, [4]SRON Space Research Organisation Netherlands, Leiden, The Netherlands, [5]Department of Atmospheric Science, Colorado State University, Fort Collins, CO, USA, [6]Now at Department of Atmospheric and Earth Science, The University of Alabama in Huntsville, Huntsville, AL, USA

Abstract This paper describes improvements to geophysical retrievals from NASA's Advanced Microwave Precipitation Radiometer (AMPR) during the Cloud, Aerosol and Monsoon Processes Philippines Experiment (CAMP^{2}Ex). The retrieved products are validated using independent data sets, and example applications in addressing science questions about the maritime tropics are provided. Multi-linear regression equations previously developed to retrieve cloud liquid water path (CLW), total precipitable water vapor (WV), and 10-m wind speed (WS) from AMPR brightness temperatures in the midlatitudes were examined. Initial testing revealed that the CLW methods required modification for the maritime tropics, likely due to the stark environmental differences. Minor WS adjustments were also needed to account for the presence of a new AMPR radome. Compared with numerical simulations, the updated CLW equation performed nearly an order of magnitude better than its predecessor. Validating AMPR CLW with airborne polarimeter-derived CLW throughout CAMP^{2}Ex yielded a median absolute deviation that is less than the predecessor CLW equation's uncertainty and comparable to CLW precisions observed in past studies. In situ WV and WS validation using dropsondes was promising, with mean deviations that are less than their target uncertainties. Correlating AMPR CLW with polarimeter-derived cloud-top height (CTH) indicated an expected CLW $\propto$ CTH^2 relation for CTH < 4 km, but reduced CLW for CTH > 4 km may have been associated with cloud droplet removal via accretion and/or mixed-phase onset. These results demonstrate the power of airborne radiometer geophysical retrievals as standalone metrics and the insight they provide when used alongside other data sets.

Plain Language Summary This study focused on retrieving quantitative cloud liquid water, atmospheric water vapor, and near-surface wind speeds over the ocean using an airborne microwave remote-sensing instrument from a 2019 NASA field campaign around the Philippines. After updating the cloud liquid water method for the tropical marine environment, all three products were compared against retrievals from other airborne instruments, and the resulting differences for each product were within targeted ranges. Transformations of cloud water into rain and/or ice were also apparent. These results are important as they indicate the potential utility of these retrieval methods in broader airborne and spaceborne studies, such as those investigating the two-way interactions between environmental conditions and convection along with their associated local and larger-scale impacts.

1. Introduction

Airborne geophysical retrievals yield critical insight into Earth's atmosphere processes and surface characteristics and are often used to inform global satellite-based analyses. The National Aeronautics and Space Administration (NASA) Advanced Microwave Precipitation Radiometer (AMPR) has provided invaluable geophysical information throughout 25+ airborne field campaigns. Horizontally (H) and vertically (V) polarized brightness temperatures (T_b) can be deconvolved from mixed-polarization T_b across AMPR's entire swath, enabling retrievals of geophysical parameters such as cloud liquid water path (CLW), total precipitable water vapor (WV), and 10-m wind speed (WS) over water surfaces (Amiot et al., 2021; hereafter "AM21"). With broad applications

Methodology: Corey G. Amiot, Timothy J. Lang, Bastiaan van Diedenhoven, Susan C. van den Heever, Lawrence D. Carey
Project administration: Timothy J. Lang
Resources: Timothy J. Lang, Lawrence D. Carey
Software: Corey G. Amiot, Timothy J. Lang
Supervision: Timothy J. Lang
Validation: Corey G. Amiot
Visualization: Corey G. Amiot
Writing – original draft: Corey G. Amiot, Timothy J. Lang, Bastiaan van Diedenhoven, Lawrence D. Carey, Sean W. Freeman, G. Alexander Sokolowsky
Writing – review & editing: Corey G. Amiot, Timothy J. Lang, Bastiaan van Diedenhoven, Susan C. van den Heever, Sean W. Freeman

for scientific analyses and instrument validations across numerous past, present, and future airborne and spaceborne missions, reliable AMPR-based retrievals are essential.

AMPR participated in NASA's Cloud, Aerosol and Monsoon Processes Philippines Experiment (CAMP^{2}Ex), which focused on interactions between aerosols, radiation, and clouds in the maritime tropics (Reid et al., 2023). NASA's P-3B Orion (P-3) aircraft conducted 19 research science flights (SFs) from Clark International Airport during 20 August–10 October 2019, covering numerous geographical, synoptic, mesoscale, aerosol, and radiation conditions (Reid et al., 2023). Locations of AMPR's CAMP^{2}Ex retrievals are provided in (Figure S9 in Supporting Information S1). Alongside AMPR, other P-3 instruments important for this study include the Advanced Vertical Atmospheric Profiling System (AVAPS) and Research Scanning Polarimeter (RSP).

Wilheit and Chang (1980), Wentz and Spencer (1998), and Hong and Shin (2013) retrieved geophysical parameters (e.g., CLW, WV, and WS) using emitted and scattered radiation properties at different microwave frequencies (e.g., Wentz & Meissner, 2000), which compare favorably with simulations (e.g., Hwang et al., 2019; Yeh et al., 1990; Zhou et al., 2013) and observations (e.g., Cecil & Biswas, 2017; McGrath & Hewison, 2001; Wentz, 1997). Spencer et al. (1994), Hood et al. (2006), and Amiot (2023) applied these principles to AMPR, while AM21 developed and tested multi-linear regression equations for CLW, WV, and WS in the Olympic Mountains Experiment and Radar Definition Experiment (OLYMPEX/RADEX; Houze et al., 2017). These retrievals can be powerful, but such methods are often necessarily tuned to a specific set of frequencies and may only perform optimally under relatively limited conditions and/or climate regions. For example, methods developed for the midlatitudes may not properly account for environmental differences when applied in the tropics, necessitating retrieval updates (e.g., Wentz & Spencer, 1998).

Satellite-retrieved cloud optical thickness (COT) and cloud-top droplet effective radius can be used to derive CLW assuming an adiabatic vertical profile of cloud droplet growth after cloud condensation nuclei are activated near the non-precipitating cloud base (Bennartz, 2007; Miller et al., 2016). This assumed profile implies that cloud liquid water content scales linearly with cloud-top height (CTH), and integration yields CLW $\propto$ CTH^2. However, some cloud processes (e.g., entrainment, evaporation, collision-coalescence) are not fully represented by these assumptions (Bennartz, 2007; Miller et al., 2016).

Though dependent on synoptic patterns and mesoscale features (e.g., cold pools), mean tropical maritime background wind speeds are ∼6–8 m s^{-1} (West & Smith, 2021) with a water-vapor-rich boundary layer (e.g., Tompkins, 2001). Tropical environmental 0°C level is often ∼5 km AMSL (e.g., Fierro et al., 2012; Zipser & LeMone, 1980), providing relatively deep warm-phase clouds (e.g., Mülmenstädt et al., 2015). Cumulus-type clouds may have considerable CLW > 0.1 kg m^{-2}, though lower CLW values are most common (e.g., Ackerman, 1959; Oh et al., 2018; O'Dell et al., 2008).

The purposes of this study are: (a) apply, update, and validate AMPR's geophysical retrievals in maritime tropical environments; and (b) demonstrate the retrievals' scientific utility (e.g., to CAMP^{2}Ex's science questions). In the latter, we explore AMPR's tropical retrieval statistics along with cloud and precipitation processes inferred from CLW retrievals. These results have broader applications and support for missions other than CAMP^{2}Ex, including past (for example, Tropical Rainfall Measuring Mission (TRMM) Microwave Imager (Kummerow et al., 1998)), present (for example, Global Precipitation Measurement (GPM) Microwave Imager (Skofronick-Jackson et al., 2017)), and future (for example, Atmosphere Observing System (AOS) mission (Atmosphere Observing System, 2022)) platforms with similar frequencies.

Data and methods are provided in Section 2, with discussions of AMPR's updated retrievals in Section 3 and example science applications in Section 4. Section 5 concludes with a summary and future work.

2. Materials and Methods

2.1. Data

All data (Aknan & Chen, 2020) were from CAMP^{2}Ex SFs 05–19; AMPR was inoperable during SF 01, and some AMPR gains and offsets were unoptimized in SFs 02–04 (Lang et al., 2021). AMPR scans cross-track ±45° from aircraft nadir, yielding mixed-polarization T_b values at four central frequencies/channels: 10.7, 19.35, 37.1, and 85.5 GHz (Spencer et al., 1994) in 50 pixels per scan, wherein footprint resolution varies with aircraft altitude. The AMPR-retrieved T_b accuracy during CAMP^{2}Ex was approximately ±1 K (Spencer et al., 1994; AM21).

Noted in Section 1, AMPR T_b can be deconvolved into pure H and V components (AM21). AMPR pixels were masked for: (a) P-3 pitch or roll magnitude ≥2°, (b) AMPR's nadir-stare mode, (c) P-3 GPS altitude <3 km, (d) scans that included at least one pixel over land (though other AMPR retrievals are possible over land, such as ice water path; McMurdie et al., 2022), and/or (e) precipitation present within the pixel. Explanations for these masks are provided in Lang et al. (2021), but to summarize, excess pitch/roll magnitudes and nadir-stare mode were masked due to AMPR's retrieval regression coefficients being tied to Earth incidence angle and assuming level flight (AM21). AMPR's cold calibration target is cooled using ambient air, leading to data quality issues in warmer air below 3 km AGL during CAMP^{2}Ex. The retrievals herein are based on atmospheric properties over an ocean background and become invalid over land and in precipitation. P-3 altitude ranged from ∼3 to 7 km AGL herein, yielding AMPR cross-track footprint resolutions of ∼94–220 m.

Of the 154 AVAPS dropsondes from SFs 05–19 (Vömel et al., 2020), three were removed due to lack of corresponding AMPR data during their descent (e.g., repeated aircraft maneuvers), one (two) from SF 08 (SF 14). Another seven were removed during quality control (e.g., unavailable near-surface winds), leaving 144 dropsondes. Two-Hz AVAPS pressure, temperature, relative humidity, and horizontal wind uncertainties are ±0.5 hPa, ±0.2°C, ±3%, and ±0.5 m s^{-1}, respectively (Freeman et al., 2020).

RSP (Cairns et al., 1999) measures I, Q, and U Stokes parameters at nine wavelengths in the visible and shortwave infrared spectrums while scanning 105° along track. RSP's spatial resolution is ∼14 mrad or ∼10–100 m depending on distance between aircraft and cloud top. Multi-angle polarimetric data at ∼865-nm wavelength are used to infer cloud-top effective radius and effective variance using the cloudbow approach (Alexandrov et al., 2012). COT is inferred from nadir observations near 865 nm (Sinclair et al., 2021). CTH values in Section 4 are inferred using a multi-angle parallax method and have an estimated accuracy within 500 m (Sinclair et al., 2017).

2.2. Methods

AMPR's geophysical retrieval equation developments are detailed in AM21 and briefly overviewed herein. Following Biswas et al. (2017), 523,176 globally distributed Global Data Assimilation System (GDAS; NCEP, 2000) profiles were used to create a physical T_b data set, which was applied to the GPM Intercalibration Working Group's oceanic radiative transfer model (Biswas et al., 2013) to simulate AMPR-observed T_b in the same scenes. This radiative transfer model incorporates climatological cloud heights (Wisler & Hollinger, 1977), with additional details in Biswas et al. (2013). Since GPM has frequency overlap with AMPR, this model is well-suited for simulating AMPR's retrievals. In these formulations, WS and sea surface temperature (SST) were randomly varied from 0 to 20 m s^{-1} and 0–30°C, respectively, to decouple the ocean and atmosphere, and 0.5 K of Gaussian noise associated with input T_b measurement error was introduced to maintain model stability. Using this physical T_b data set, AMPR-observed T_b was simulated every 0.2° Earth incidence angle between 0° and 50°. In these simulations, Rosenkranz models for nitrogen, oxygen, water vapor, and cloud liquid water were used to calculate atmospheric absorption coefficients (Liebe et al., 1991; Rosenkranz, 1993; Rosenkranz, 1998; AM21). Multi-linear regression was performed on the resulting data to produce the AM21 CLW, WV, and WS equation forms. Numerous AMPR channels and formulations were examined in sensitivity tests for each parameter, and residual errors (Mathworks, 2025) were analyzed to select the equation form with the lowest retrieval and crosstalk errors for each parameter. Further, following AM21, AMPR T_b were corrected for biases in observed T_b compared to GDAS-simulated T_b on a flight-by-flight basis for all analyses herein; these corrections are exemplified in the bottom four rows of Figure 1.

Following their development, AM21's retrieval equations, displayed in Section 3 and compared with the updated retrieval methods herein, were applied to AMPR's CAMP^{2}Ex data; an example is provided in Figure 1's left column. During the SF 09 segment in Figure 1, WV appears uniform with reasonable values for the maritime tropics (that is, background of ∼50 kg m^{-2}; second row). Thus, AM21's WV retrieval methods were deemed valuable for maritime tropical use, as were the underlying methods used to develop the equations as discussed in the preceding paragraph. However, two issues are apparent in Figure 1's left column: 1) clear-air CLW around 0.1 kg m^{-2} (first row), and 2) cross-track WS stripes (i.e., periodic WS variations across AMPR's swath; third row), which are visible in clear air around 0311–0312 UTC. These features appeared throughout CAMP^{2}Ex, and it was concluded that the AM21 CLW retrieval equation would require updating while post-retrieval smoothing of AM21 WS artifacts would be necessary for CAMP^{2}Ex; these retrieval modifications are presented in this paper.

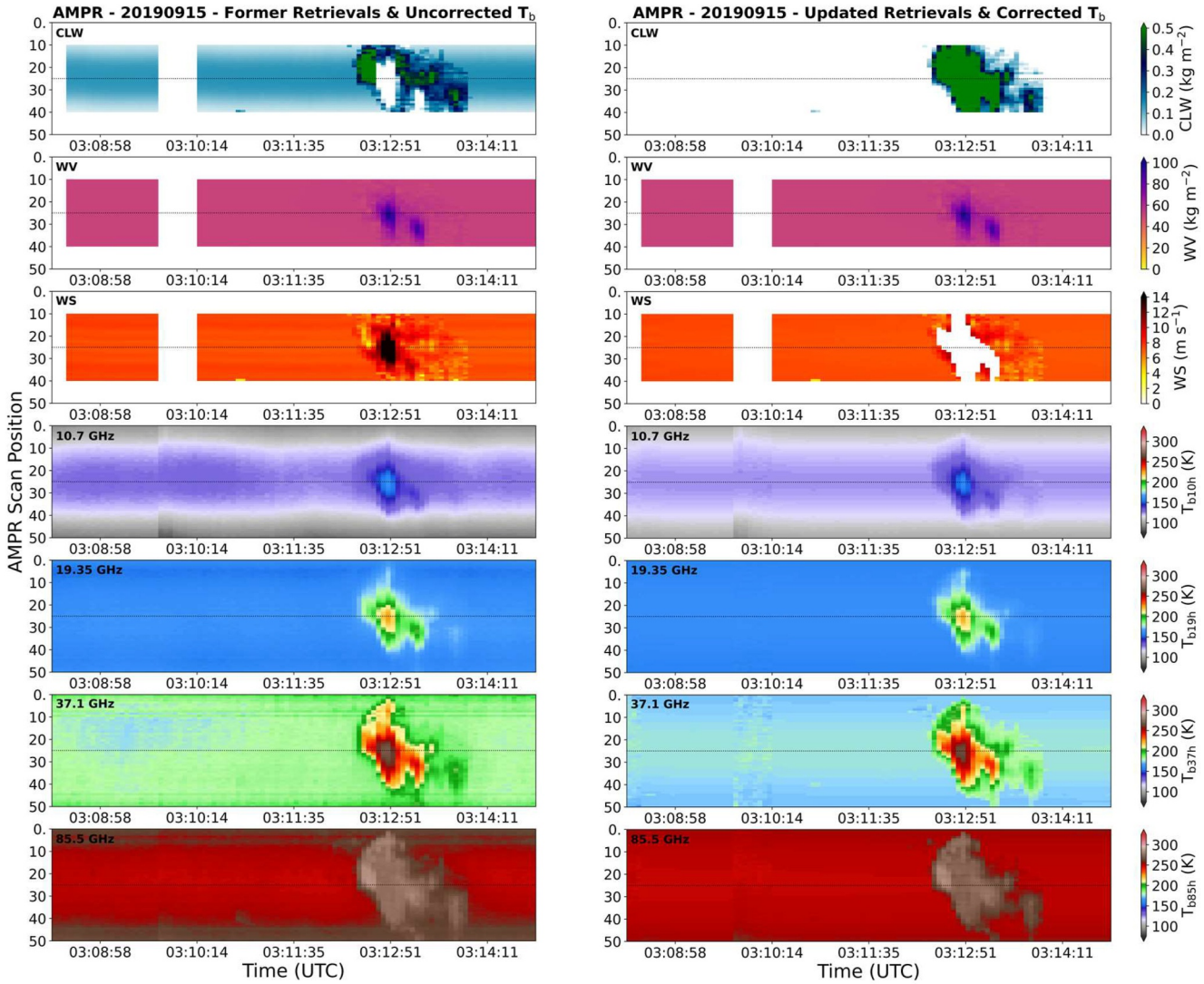

Figure 1. Strip charts (i.e., top-view time series) of Advanced Microwave Precipitation Radiometer (AMPR) data and retrievals from approximately 0308–0314 UTC during science flight 09. From top to bottom, plots in each column are of: AMPR's CLW, WV, and wind speed (WS) retrievals and deconvolved H polarized T_b at 10.7, 19.35, 37.1, and 85.5 GHz. The left column presents retrievals from direct application of the AM21 equations, along with uncorrected T_b. The right column presents updated CLW via Equation 2 and smoothed WS (Figure S10 in Supporting Information S1), along with corrected T_b. WV retrievals are the same in both columns. Nadir is indicated by each black dotted line. AMPR's precipitation flag is demonstrated in the WS retrievals (right column) around 0313 UTC. Retrievals are masked in the 10 scan positions nearest swath edges due to residual radome effects, and retrievals are masked around 0310 UTC due to aircraft maneuvers.

The aforementioned high clear-air CLW likely resulted from high water vapor, while cross-track stripe artifacts were likely caused by AMPR's radome amplifying any cross-track variations present in the retrieval equations. Prior to CAMP^{2}Ex, a new flat-surface radome was custom built out of Rexolite (http://www.rexolite.com) by ProSensing Inc. to be P-3 compatible and optimized for AMPR's frequencies, which introduces an insertion loss that varies with incidence angle and frequency (Lang et al., 2021). As discussed below and in Supporting Information S1, WS stripes were smoothed by applying simple offsets to AM21's equation output while an entirely new CLW equation was created and tested, after which bulk AMPR retrieval statistics were computed.

Once the final retrieval equation forms were selected and applied throughout CAMP^{2}Ex, the results were validated with independent measurements. For comparisons with AMPR-derived WV and WS, total precipitable water and 10-m WS were calculated from the 144 dropsondes using the equations from AMS (2019) and Uhlhorn et al. (2007) referenced in AM21. AMPR-retrieved WV and WS were averaged during each dropsonde descent's entirety to reduce influences from noise and non-precipitating clouds (AM21). Percentage (absolute) differences

between AMPR-derived and AVAPS-calculated "truth" values were used to evaluate AMPR's WV (WS) retrievals.

Validating AMPR's CLW retrievals with in situ observations proved more challenging; therefore, independent CLW values were calculated using RSP data. For consistency in viewing angle and signal paths, only directly downward-pointing nadir data were used from both instruments. Following Bennartz (2007) and Miller et al. (2016),

$$\mathrm{CLW}\left(\mathrm{g\ m^{-2}}\right) = {}^{5}\!/_{9} \cdot \rho_w \cdot \mathrm{COT} \cdot r_e, \tag{1}$$

where COT is cloud optical thickness (unitless), r_e is cloud-top effective radius (m), and ρ_w is liquid water density (g m^{-3}). Since cloud reflectance asymptotes at high optical thickness, any COT > 100 units was set to 100 units in Equation 1 to constrain CLW (Platnick et al., 2017). The AMPR scan start time nearest each RSP scan start time was determined and all concurrent AMPR and RSP CLW observations were used to calculate absolute deviations, percentage deviations, and biases. Flight-by-flight breakdowns of all retrieval validations are provided in Supporting Information S1.

3. AMPR's CAMP^{2}Ex Geophysical Retrievals

This section presents statistical performances of AMPR's maritime tropical CLW, WV, and WS retrievals. We begin with CLW development and preliminary testing against GDAS simulations before progressing to validations of each parameter using independent CAMP^{2}Ex data. Additional details are in Supporting Information S1.

3.1. Cloud Liquid Water: Development

AM21's CLW equation yielded clear-air CLW around 0.1–0.2 kg m^{-2} throughout CAMP^{2}Ex (e.g., upper-left panel in Figure 1), likely due to crosstalk error caused by its insufficient optimization to reject the microwave signature of WV, especially >20 kg m^{-2}. To mitigate this, CLW's equation format was varied in sensitivity tests (e.g., adding or removing elements and channels) and developing new multi-linear regression coefficients from the GDAS data set to separate atmospheric signal from surface signal, following AM21. In preliminary testing of equation performance, simulated AMPR CLW was compared against GDAS-output CLW, WV, WS, and SST across the 523,176 profiles by evaluating error variance from each regression analysis (Mathworks, 2025). Several "candidate" CLW equations were also compared with independent CAMP^{2}Ex data (Supporting Information S1). The goal was selecting an equation that: (a) minimized CLW retrieval and crosstalk errors, (b) yielded uniform clear-air CLW values, and (c) rarely produced negative values beyond the retrieval root-mean-square deviation (RMSD).

The selected CLW retrieval equation was:

$$\begin{aligned}\mathrm{CLW}\left(\mathrm{kg\ m^{-2}}\right) = {} & a_0 + a_1 T_{b19v} + a_2 T_{b19h} + a_3 \ln(290 - T_{b19v}) + a_4 \ln(290 - T_{b19h}) + a_5 T_{b37v} + a_6 T_{b37h} \\ & + a_7 \ln(290 - T_{b37v}) + a_8 \ln(290 - T_{b37h}) + a_9 T_{b85v} + a_{10} T_{b85h} + a_{11} \ln(295 - T_{b85v}) \\ & + a_{12} \ln(295 - T_{b85h}) + a_{13}\mathrm{SST},\end{aligned} \tag{2}$$

where "a" terms are (unitless) regression coefficients for Earth incidence angle every 0.2° (see in Supporting Information S1), $T_{bxxh,v}$ represents T_b (K) at xx-GHz frequency and H or V polarization, and SST is in K. Applying Equation 2 to the same AMPR data yielded lower clear-air CLW and much greater cross-track uniformity; however, slight residual clear-air CLW remained throughout each flight (see Figure S2 in Supporting Information S1). To mitigate this, the average CLW across all "clear-air" AMPR pixels was calculated for each flight (see Figure S5 in Supporting Information S1), and this value was subtracted from CLW in every AMPR pixel throughout the respective flight. "Clear air" was defined as any AMPR pixel wherein 85.5-GHz T_b was less than the average 85.5-GHz T_b among all unmasked AMPR pixels during the flight, which would predominantly reside in clear air. Negative CLW resulting from this mitigation was set to 0 kg m^{-2}, which impacts error statistics discussed below. Other equations were examined during sensitivity testing (Supporting Information S1) but they: (a) did not compare as favorably with GDAS as Equation 2, (b) had significant clear-air cross-track variability, and/or (c) frequently yielded negative CLW outside the retrieval RMSD, as presented below.

The use of Equation 2 improved AMPR's tropical CLW retrievals compared to the AM21 method via three main differences: (a) 37.1-GHz T_b; (b) linear equation elements; and (c) a background SST value. AMPR's 37.1-GHz channel is more (less) susceptible to attenuation compared to 19.35 (85.5) GHz, offering greater insight about the CLW profile in a given water-vapor-rich tropical cloud. Linear equation elements appeared to improve retrievals, possibly by helping establish general regression data trends (e.g., CLW increases associated with T_b increases) despite the highly nonlinear relationship between T_b and CLW. In Equation 2, a single median SST from the GDAS simulation and pixel nearest the middle of the SF was applied uniformly to all AMPR pixels throughout the flight. This inclusion does not significantly influence retrieved values but provides a background to mitigate cross-track artifacts (AM21) and appeared to assist with scaling CLW retrievals to the maritime tropics. Sea surface temperature differed by <2 K across SFs 05–19.

3.2. Cloud Liquid Water: Testing and Validation

Comparing CLW simulations (Equation 2) with GDAS values (Figure S4 in Supporting Information S1), mean CLW retrieval and crosstalk errors were roughly 0 kg m^{-2} across the ranges of geophysical values tested, with most standard deviations $<2.50 \times 10^{-2}$ kg m^{-2}. This indicates Equation 2's excellent performance across various ocean-surface and atmospheric conditions. RMSD of Equation 2's retrieval error was 1.94×10^{-2} kg m^{-2}, nearly an order of magnitude lower than in AM21 and similar to the RMSD in Wentz and Meissner (2000). Average retrieval error was 1.90×10^{-3} kg m^{-2}, and mean crosstalk errors with WV, WS, and SST were very low at 1.37×10^{-2}, 3.60×10^{-3}, and 4.79×10^{-4} kg m^{-2}, respectively. Standard deviation of CLW-WV crosstalk error increased as WV increased, reaching approximately 2.50×10^{-2} kg m^{-2} for WV > 30 kg m^{-2}, while mean CLW-WV crosstalk error remained around 0 kg m^{-2}. Based on its excellent simulation performances, Equation 2 was tested using CAMP^{2}Ex AMPR data, wherein it yielded lower residual clear-air CLW compared to the AM21 equation and cross-track variation was significantly reduced (right column of Figure 1). However, as noted previously, slight residual clear-air CLW, typically <0.05 kg m^{-2}, required additional correction, which may have been influenced by crosstalk errors (e.g., with WV).

Absolute deviations from comparing AMPR with RSP CLW were favorable with a median around 8.08×10^{-2} kg m^{-2}, which is less than the GDAS RMSD in AM21. We focus on median values given their insensitivity to outliers. Due to its fine 865-nm wavelength, RSP's sensitivity to cloud droplets produces reliable validation data for AMPR CLW. RSP percentage deviations and median biases were also low at 86.0% and -3.28×10^{-2} kg m^{-2}, respectively. Only 12 of the 1,874 data points in the AMPR-RSP comparative analysis (Figure 2) had AMPR CLW > 1 kg m^{-2}, indicating very limited rain contamination in a statistically significant data set for AMPR CLW error/deviation statistics. However, differences in instrument characteristics and retrieval methods manifest in the moderate 0.42 correlation. AMPR-RSP correlations were strongest for CLW > 3.0×10^{-2} kg m^{-2}, suggesting this might be a useful noise floor. The relatively coarse GDAS data used to train AMPR's CLW retrievals may have lower sensitivity to smaller-scale T_b variations captured in the finer-scale AMPR data, potentially enhancing errors. However, AMPR CLW retrieval performances discussed above and in AM21 demonstrate their ability to capture smaller-scale cloud features with relatively high accuracy when compared with independent observations.

3.3. Water Vapor: Validation

AM21's WV retrieval method performed well against in situ observations (Figure 2). Overall mean difference between AMPR- and AVAPS-derived WV was 8.27%, which is less than the 10% target uncertainty (National Academies of Sciences, Engineering, and Medicine (NASEM), 2018) despite AMPR occasionally yielding higher WV than AVAPS. Flight-average WV differences were <10% for all but two SFs (Figure S7 in Supporting Information S1). Cross-track WV stripe artifacts (AM21) did not appear during CAMP^{2}Ex (Figure 1). Therefore, AMPR's WV retrieval equation was left unchanged from AM21:

$$\begin{aligned}\mathrm{WV}\left(\mathrm{kg\ m^{-2}}\right) = {} & a_0 + a_1 T_{b10v} + a_2 T_{b10h} + a_3 \ln(290 - T_{b19v}) + a_4 \ln(290 - T_{b19h}) + a_5 \ln(290 - T_{b37v}) \\ & + a_6 \ln(290 - T_{b37h}) + a_7 \mathrm{SST}, \end{aligned} \quad (3)$$

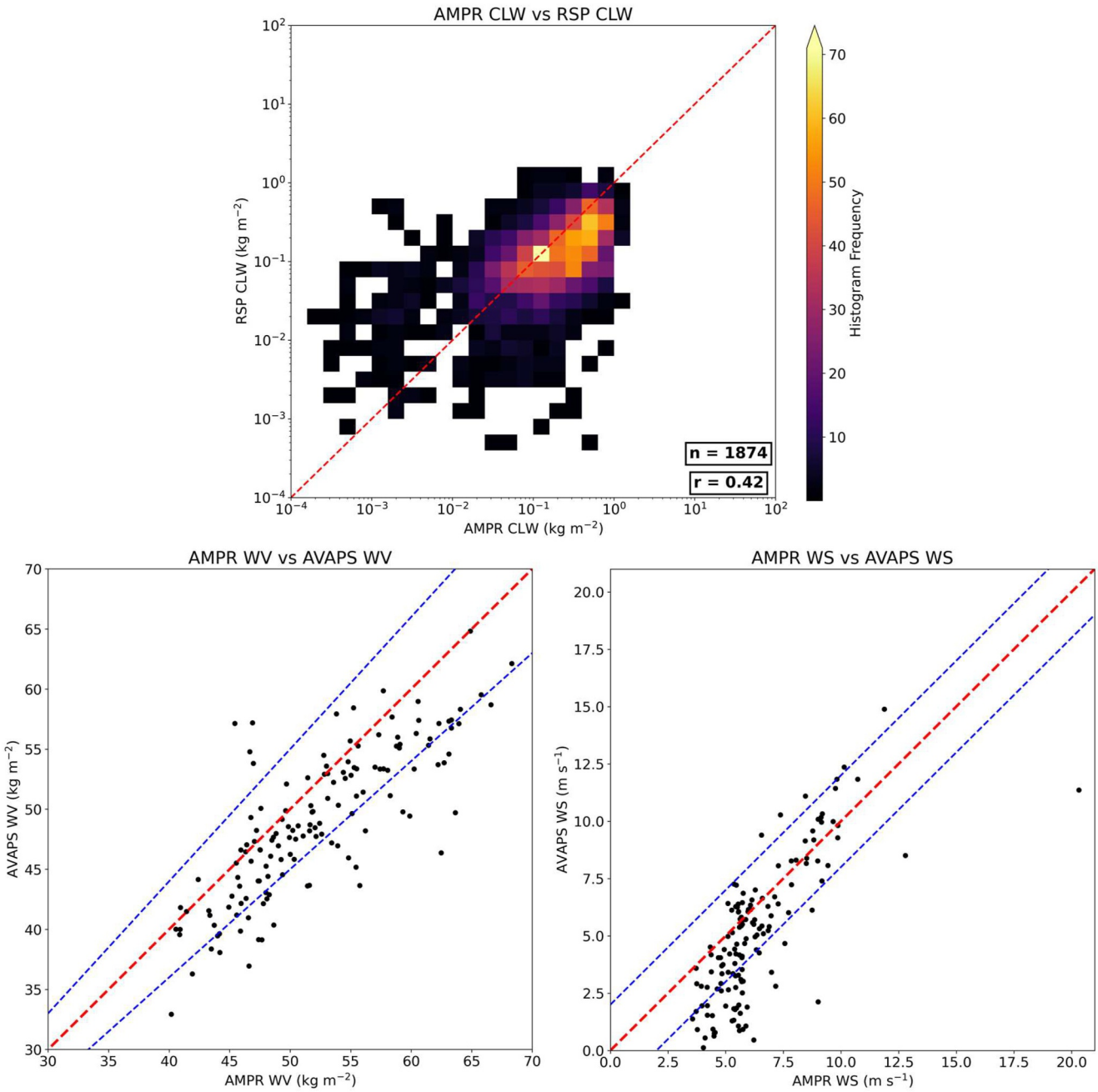

Figure 2. Top: two-dimensional histogram (with logarithmic axes) comparing Advanced Microwave Precipitation Radiometer (AMPR) CLW with Research Scanning Polarimeter (RSP) CLW for all unmasked coincident downward-pointing nadir AMPR and RSP observations, with number of coincident observations (n) and Pearson correlation coefficient (r) also displayed. Bottom: scatterplots of WV (left) and wind speed (WS) (right) retrieved using AMPR (*x* axes) and Advanced Vertical Atmospheric Profiling System (*y* axes) data. Red dashed lines denote a one-to-one ratio. Blue dashed lines encompass the target maximum difference of ±10% (±2 m s^{-1}) for WV (WS).

where each term follows Equation 2's definitions. The excellent agreement between Equation 3 and AVAPS is interesting considering climatological differences between OLYMPEX/RADEX and CAMP^{2}Ex. Excluding 85.5-GHz data from Equation 3 likely mitigated influences from water vapor differences between these regions, and background GDAS SST may have assisted with scaling WV retrievals to the maritime tropics, as noted in Section 3.1.

3.4. Wind Speed: Testing and Validation

AMPR's WS retrievals required relatively minor updates for CAMP^{2}Ex, which suggests that using linear, logarithmic, and exponential terms to model the nonlinear relationship between T_b and WS in AM21 was relevant for wind-induced effects on T_b in the tropics, in addition to background information provided by the SST term as noted previously. AM21's WS equation provided excellent agreement with in situ observations, with a mean AMPR-AVAPS difference of 1.81 m s^{-1} across SFs 05–19, which is less than the 2 m s^{-1} target uncertainty (Ruf et al., 2019; Wentz & Meissner, 2007):

$$\begin{aligned}\mathrm{WS}\left(\mathrm{m\ s^{-1}}\right) = {} & a_0 + a_1 \ln(285 - T_{b10v}) + a_2 \ln(285 - T_{b10h}) + a_3 T_{b10v}^2 + a_4 T_{b10h}^2 + a_5 (T_{b10v} T_{b10h}) \\ & + a_6 T_{b19v} + a_7 T_{b19h} + a_8 T_{b19v}^2 + a_9 T_{b19h}^2 + a_{10} (T_{b19v} T_{b19h}) + a_{11} T_{b37v} + a_{12} T_{b37h} \\ & + a_{13} T_{b37v}^2 + a_{14} T_{b37h}^2 + a_{15} (T_{b37v} T_{b37h}) + a_{16} \mathrm{SST}, \end{aligned} \tag{4}$$

where each term follows Equation 2's definitions. However, cross-track stripe artifacts were present (Figure 1); relatively consistent patterns indicate possible attribution to AMPR's radome and associated transmission loss varying with incidence angle and frequency. To account for this, a median WS offset was calculated for each scan position throughout each SF (Figure S10 in Supporting Information S1). In these calculations, the difference between WS in each pixel within an AMPR scan and the median WS from the same scan was calculated, and the overall median of these differences throughout the SF was calculated for each scan position. Most offset magnitudes were <0.5 m s^{-1} apart from SF 18 which largely took place over/near land. These variations may also be partially attributable to residual WS retrieval error and T_b variation in subsequent scan positions amplified by squared functions in Equation 4. Cross-track maxima and minima were at similar positions for all SFs in Figure S10 in Supporting Information S1, exemplifying some cross-track sensitivity of Equation 4 that were potentially amplified by AMPR's radome; thus, Equation 4 may be applicable to other radiometers without adjustment.

After smoothing retrieved WS using the values in Figure S10 in Supporting Information S1, they were validated using the 144 dropsondes. The adjustments slightly improved AMPR-AVAPS WS differences, yielding a CAMP^{2}Ex-average difference of 1.76 m s^{-1}. This indicates excellent agreement and is less than the 2 m s^{-1} target uncertainty. Flight-average WS differences were <2 m s^{-1} in 11 of 15 SFs (Figure S7 in Supporting Information S1). It should be mentioned that AMPR tended to yield higher WS than AVAPS for wind speeds <∼5 m s^{-1} and AMPR WS values <3.5 m s^{-1} were not observed in the AMPR-AVAPS comparison data set (Figure 2). Increased uncertainty in AMPR WS at lower wind speeds matches AM21, largely due to minimal wind-induced surface emissivity increases (e.g., Wilheit & Chang, 1980). However, AMPR's overestimations of WS under these conditions are unexpected, since AM21 noted a general underestimation in AMPR WS for wind speeds <5 m s^{-1}. Since WS < 3.5 m s^{-1} were observed during OLYMPEX/RADEX in AM21, it is possible that higher SSTs during CAMP^{2}Ex decreased the retrieval's sensitivity to WS < 3.5–5 m s^{-1}. Further examination of this trend is needed, but it should be noted that AMPR agreed exceptionally well with AVAPS for WS > 3.5–5 m s^{-1}. This indicates that AMPR WS retrievals are useful and reliable, especially when considering that mean maritime tropical surface wind speeds are ∼6–8 m s^{-1} (West & Smith, 2021) and many mesoscale processes (e.g., cold pools) further increase WS locally.

4. Example Science Applications

This section focuses on applying AMPR's retrievals in preliminary CAMP^{2}Ex science analyses. An overview of AMPR's retrieval statistics is presented first and followed by discussion of AMPR CLW versus RSP-derived CTH.

4.1. Bulk AMPR Retrieval Statistics

Statistics for AMPR's retrievals are presented in Figure 3, wherein median CLW, WV, and WS values are shown since slight residual T_b enhancements near precipitation affected mean values. The median and mode CLW were around 0 kg m^{-2} with a relatively smooth decrease in histogram frequency as CLW increased. The latter matches expectations (Ackerman, 1959; Oh et al., 2018), while the mode and median around 0 kg m^{-2} likely resulted from prevalent clear-air pixels and removal of negative CLW values as discussed in Section 3. Mean CLW outside of precipitation-flagged regions was 0.07 kg m^{-2}, which is within the range of values expected in the maritime tropics

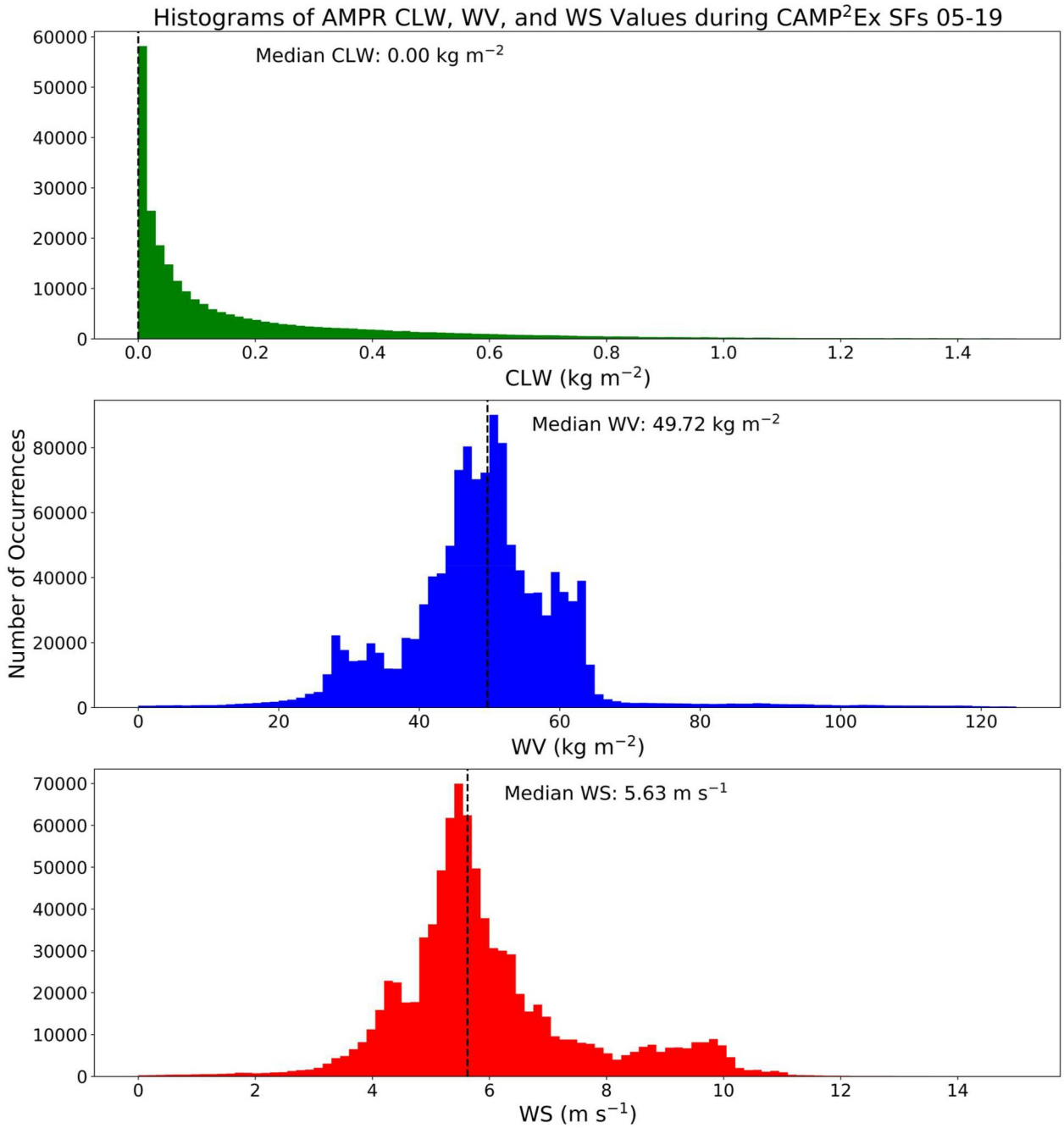

Figure 3. Histograms of precipitation-masked Advanced Microwave Precipitation Radiometer cloud liquid water path (top), water vapor (middle), and wind speed (bottom) retrievals.

(Greenwald et al., 1995). Setting negative CLW to 0 kg m^{-2} creates a slight positive bias in the statistics and may contribute to residual calculated clear-air CLW values noted in Supporting Information S1. A separate analysis (not shown) of all unmasked AMPR pixels produced a histogram that was fairly evenly distributed about a near-zero mode of 1.94×10^{-2} kg m^{-2}, which is within the CLW RMSD and indicates low bias in the CLW retrievals via Equation 2. Minimum (maximum) mean CLW was 3.44×10^{-3} kg m^{-2} (0.223 kg m^{-2}) in SF 18 (SF 11).

The AMPR WV histogram mode and median were approximately 50 kg m^{-2} and 49.7 kg m^{-2}, respectively, which agree well with increased background WV expected in the maritime tropics compared to wintertime midlatitudes. For example, in AM21, background WV was generally less than 20 kg m^{-2}. In contrast, most

CAMP^{2}Ex WV observations were between 20 and 65 kg m^{-2}. Minimum (maximum) WV median was 42.6 kg m^{-2} (62.7 kg m^{-2}) in SF 17 (SF 10). Finally, AMPR's median WS was 5.63 m s^{-1} with a similar mode, agreeing with the 6.12 m s^{-1} mean WS around the central Pacific in West and Smith (2021). In Figure 3, WS followed a relatively uniform distribution about the median except for a cluster around 8.25–10 m s^{-1}. Flight-by-flight analyses (not shown) indicated that median WS for SFs 06 and 10 were around 8.5–9 m s^{-1}, likely due to synoptic conditions during both flights and sampling of a large cold pool throughout SF 10. Most background WS values were 3–11 m s^{-1}. Minimum (maximum) WS median was 3.95 m s^{-1} (8.77 m s^{-1}) in SF 18 (SF 10).

4.2. AMPR CLW With Respect to RSP CTH

This subsection details two analyses of AMPR-retrieved CLW as a function of RSP-derived CTH, one with AMPR's precipitation masks applied and another without these masks. A common trend is present in both analyses (Figure 4), where CLW generally increased in a manner roughly proportional to CTH^2 for CTH < 4 km AMSL. Given that liquid water content increases linearly with CTH (Miller et al., 2016), this CLW $\propto$ CTH^2 relation follows expectations. However, once CTH passes 4 km AMSL, there is considerable clustering of data points around lower CLW, especially in the precipitation-masked scatterplot. AMPR's CLW retrieval tends to fail in heavier precipitation due to higher T_b associated with enhanced emission yielding negative values in the natural logarithm term(s) in the CLW regression equation, resulting in their masking as an undefined real value (AM21). However, these retrievals provide CLW information just outside of the precipitation core where emission from cloud and lighter precipitation is comparatively lower. As a result, the data in Figure 4 are primarily from cloud water in both scatterplots. Thus, it is unexpected that data clustering would occur around lower CLW in association with high CTH.

One possible explanation is accretion and/or freezing onset in the mixed-phase region. Once clouds grew deeper, increased accretion efficiency would result in transition of liquid water from being entirely cloud water to a mixture of cloud and rain water within the same column. Since AMPR CLW and RSP are not as sensitive to rain water as cloud water, these products would not display the rain water portion well but would continue to capture the cloud water portion during this transition. This would decrease CLW despite the increased CTH. Likewise, freezing of lofted cloud droplets would transition liquid water to ice water, reducing CLW (all else being equal). These ice processes become increasingly significant around 5 km AMSL, a common tropical freezing level (Fierro et al., 2012; Zipser & LeMone, 1980). This is potentially important as it suggests that conversion of cloud water to rain and/or ice water became significant in CAMP^{2}Ex's maritime tropical environment once CTH increased past ∼4 km AMSL. Cloud droplet effective radii (Figure 4) were not anomalously large in these ice-processes regions, which suggests minimal influence of any smaller ice hydrometeors (i.e., <30 μm) on CLW retrievals via Equation 1; this further indicates the reliability of RSP CLW for validating AMPR CLW.

There were instances where stratocumulus cloud layers impacted RSP CTH–the mid-level cloud layer was reported as CTH, but the relatively shallow layer yielded comparatively low CLW. To address this, data (Figure 4) were split into "low" and "high" COT groups using a threshold of 15 units (Fu et al., 2022). While several low-CLW/high-CTH data points were associated with thin clouds, many were associated with optically thick clouds. Therefore, the unexpected CLW decrease with increasing CTH persisted in some thicker clouds. However, spatial matching of CLW-CTH data pairs may have been affected by differences in AMPR (94–220 m) and RSP (∼10–100 m) spatial resolutions. This is especially noteworthy when the P-3 passed slightly to the side of a cloud, which AMPR could have captured while RSP missed it. Additionally, slight AMPR-RSP temporal offsets (e.g., ∼1 s in corresponding downward-pointing data) due to their scan durations may have led to some mismatched sampling. Thus, further investigation into this relation, including other cloud patterns (e.g., multiple cloud layers) is warranted.

5. Summary and Future Work

This paper demonstrated AMPR's geophysical retrieval capabilities in the maritime tropics and were uniquely performed through AMPR's new custom radome. Applying retrieval methods previously developed for the midlatitudes (AM21) indicated that AM21's WV method was suitable for the maritime tropics while WS stripe artifacts and residual clear-air CLW were present. To mitigate these, a new CLW equation was formulated, and corrections were developed for CLW and WS. The new CLW equation agreed well with GDAS simulations, with RMSD of 1.94×10^{-2} kg m^{-2}, mean retrieval error of 1.90×10^{-3} kg m^{-2}, and crosstalk errors with WV, WS, and

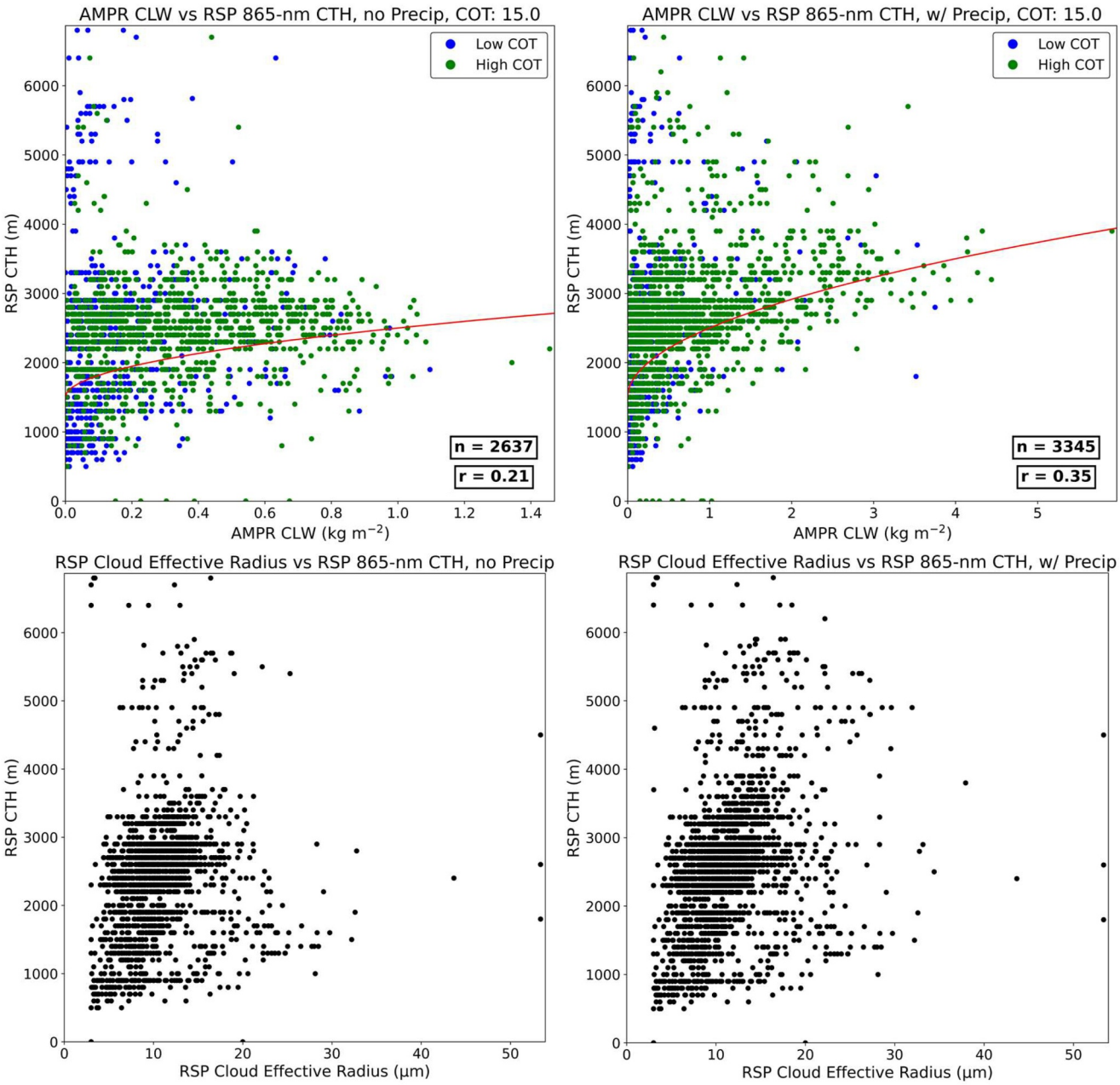

Figure 4. Scatterplots of Advanced Microwave Precipitation Radiometer (AMPR) CLW (top row) and Research Scanning Polarimeter (RSP) cloud droplet effective radius (bottom row) versus RSP cloud-top height (CTH) (*y* axes) across all coincident data points with (left) and without (right) AMPR's precipitation flags applied. Blue (green) data points in the top row represent those wherein RSP-derived cloud optical thickness was ≤15 units (>15 units). RSP data are reported in 100-m bins. A representative red CLW $\propto$ CTH^2 line is shown in each top-row plot along with number of data points (n) and Pearson correlation coefficient (r). *X*-axis ranges differ between plots.

SST of 1.37×10^{-2}, 3.60×10^{-3}, and 4.79×10^{-4} kg m^{-2}, respectively. When applied to CAMP^{2}Ex AMPR data, the updated equation significantly reduced residual CLW and mitigated clear-air cross-track variations. AMPR's CLW median absolute deviation was relatively low at 8.08×10^{-2} kg m^{-2} when validated with RSP-derived CLW, which is less than the AM21 CLW's theoretical uncertainty, with favorable percentage deviation and median bias of 86.0% and -3.28×10^{-2} kg m^{-2}, respectively. RSP's sensitivity to cloud droplets combined with a statistically significant sample and minimal precipitation contamination provide reliable indicators of AMPR's CLW retrieval performances. The adjusted WS equation yielded 1.76 m s^{-1} mean difference when compared against 144 AVAPS dropsondes, which is less than the 2 m s^{-1} target uncertainty. Similarly, AMPR's WV

retrievals differed from AVAPS-derived values by 8.27% on average, which is less than the 10% target uncertainty. AMPR's retrievals have broad applications across many past, present, and future airborne and spaceborne missions, including TRMM, GPM, and AOS.

These retrievals were applied to CAMP^{2}Ex science objectives via two analyses: (a) bulk AMPR retrieval statistics, and (b) correlating AMPR CLW with RSP CTH. Mean CLW, median WV, and median WS outside of precipitation-flagged regions were 0.07 kg m^{-2}, 49.7 kg m^{-2}, and 5.63 m s^{-1}, respectively, which follows expectations for the maritime tropics. Correlating AMPR CLW with RSP-derived CTH yielded an expected CLW $\propto$ CTH^2 trend for CTH < 4 km AMSL. Once CTH increased past 4 km AMSL, CLW decreased considerably, which may indicate accretion and/or mixed-phase onset.

Future work will apply AMPR's retrievals to additional CAMP^{2}Ex science questions. Incorporating modeling data to fill observational gaps could be beneficial. Additional CLW validation (e.g., from airborne radar) could be considered, and examining dropsonde profiles with simulated clouds may bolster CLW results. Other updates to CLW retrieval methods, such as producing region-specific equations and utilizing neural networks, may be beneficial. Examining potential accretion/mixed-phase identification in AMPR-CLW/RSP-CTH more closely could provide useful verification of important processes in tropical convection. Developing AMPR retrievals for other geophysical parameters (e.g., surface rain rate) applicable to numerous climate regions is possible, and applying these techniques to other field campaigns will be important.

Conflict of Interest

The authors declare no conflicts of interest relevant to this study.

Data Availability Statement

All AMPR, AVAPS, and RSP data used in this study are available on the NASA Langley Research Center's Airborne Science Data for Atmospheric Composition repository at https://www-air.larc.nasa.gov/cgi-bin/ArcView/camp2ex, cited as Aknan and Chen (2020). The GDAS data are available at the National Center for Atmospheric Research's Computational and Information Systems Laboratory at https://doi.org/10.5065/D6M043C6, cited as NCEP (2000).

Acknowledgments
We are grateful to Hal Maring for financial support of AMPR's CAMP^{2}Ex deployment and data analyses. C. G. Amiot acknowledges funding from NASA Marshall Space Flight Center through Cooperative Agreement 80MSFC22M0001 with The University of Alabama in Huntsville. Manuscript revisions by C. G. Amiot were supported by an appointment to the NASA Postdoctoral Program at NASA Marshall Space Flight Center, administered by Oak Ridge Associated Universities under contract with NASA, through contract 80HQTR21CA005. S. C. van den Heever, S. W. Freeman, and G. A. Sokolowsky were supported by NASA Grant 80NSSC18K0149. Ousmane Sy, Simone Tanelli, Jay Mace, Svetla Hristova-Veleva, and Zhuocan Xu are thanked for their helpful discussions regarding AMPR's retrievals. We thank the scientists and engineers who helped prepare and support AMPR for CAMP^{2}Ex, and the anonymous Reviewers for their insightful suggestions.

References

Ackerman, B. (1959). The variability of the water contents of tropical cumuli. *Journal of Meteorology*, *16*(2), 191–198. https://doi.org/10.1175/1520-0469(1959)016<0191:TVOTWC>2.0.CO;2

Aknan, A., & Chen, G. (2020). Joint data repository – CAMP^{2}Ex, PISTON [Dataset]. NASA Langley Research Center. Retrieved from https://www-air.larc.nasa.gov/missions/camp2ex/index.html. accessed 16 November 2020.

Alexandrov, M. D., Cairns, B., Emde, C., Ackerman, A. S., & van Diedenhoven, B. (2012). Accuracy assessments of cloud droplet size retrievals from polarized reflectance measurements by the research scanning polarimeter. *Remote Sensing of Environment*, *125*, 92–111. https://doi.org/10.1016/j.rse.2012.07.012

American Meteorological Society (AMS). (2019). *Precipitable water*. AMS Glossary of Meteorology. Retrieved from http://glossary.ametsoc.org/wiki/Precipitable_water

Amiot, C. G. (2023). Airborne passive microwave geophysical retrievals and applications in assessing environmental and aerosol impacts on maritime convection. In *Ph.D. dissertation, Dept. of Atmospheric and Earth Science* (p. 176). The University of Alabama in Huntsville. Retrieved from https://louis.uah.edu/uah-dissertations/278/

Amiot, C. G., Biswas, S. K., Lang, T. J., & Duncan, D. I. (2021). Dual-polarization deconvolution and geophysical retrievals from the Advanced Microwave Precipitation Radiometer during OLYMPEX/RADEX. *Journal of Atmospheric and Oceanic Technology*, *38*(3), 607–628. https://doi.org/10.1175/JTECH-D-19-0218.1

Atmosphere Observing System (AOS). (2022). *Atmosphere observing System*. National Aeronautics and Space Administration. Retrieved from https://aos.gsfc.nasa.gov/

Bennartz, R. (2007). Global assessment of marine boundary layer cloud droplet number concentration from satellite. *Journal of Geophysical Research*, *112*(D2), D02201. https://doi.org/10.1029/2006JD007547

Biswas, S. K., Farrar, S., Gopalan, K., Santos-Garcia, A., Jones, W. L., & Bilanow, S. (2013). Intercalibration of microwave radiometer brightness temperatures for the Global Precipitation Measurement Mission. *IEEE Transactions on Geoscience and Remote Sensing*, *51*(3), 1465–1477. https://doi.org/10.1109/TGRS.2012.2217148

Biswas, S. K., Lang, T. J., Duncan, D., & Kummerow, C. (2017). *Polarization deconvolution and geophysical retrieval from a dual-pol, cross-track scanning microwave radiometer (AMPR) during OLYMPEX/RADEX. 2017 Fall Meeting*. American Geophysical Union. Abstract H32C-07 Retrieved from https://ntrs.nasa.gov/api/citations/20170012192/downloads/20170012192.pdf

Cairns, B., Russell, E. E., & Travis, L. D. (1999). Research Scanning Polarimeter: Calibration and ground-based measurements. *SPIE Proceedings, Polarization: Measurement, Analysis, and Remote Sensing II*, *3754*, 186–196. https://doi.org/10.1117/12.366329

Cecil, D. J., & Biswas, S. K. (2017). Hurricane Imaging Radiometer (HIRAD) wind speed retrievals and validation using dropsondes. *Journal of Atmospheric and Oceanic Technology*, *34*(8), 1837–1851. https://doi.org/10.1175/JTECH-D-17-0031.1

Fierro, A. O., Zipser, E. J., LeMone, M. A., Straka, J. M., & Simpson, J. (2012). Tropical oceanic hot towers: Need they be undilute to transport energy from the boundary layer to the upper troposphere efficiently? An answer based on trajectory analysis of a simulation of a TOGA COARE convective system. *Journal of the Atmospheric Sciences*, *69*(1), 195–213. https://doi.org/10.1175/JAS-D-11-0147.1

Freeman, S., Sokolowsky, G. A., & van den Heever, S. C. (2020). CAMP^{2}Ex AVAPS readme/quick start guide (p. 6). Retrieved from https://www-air.larc.nasa.gov/cgi-bin/ArcView/camp2ex

Fu, D., Di Girolamo, L., Rauber, R. M., McFarquhar, G. M., Nesbitt, S. W., Loveridge, J., et al. (2022). An evaluation of the liquid cloud droplet effective radius derived from MODIS, airborne remote sensing, and in situ measurements from CAMP^{2}Ex. *Atmospheric Chemistry and Physics*, *22*(12), 8259–8285. https://doi.org/10.5194/acp-22-8259-2022

Greenwald, T. J., Stephens, G. L., Christopher, S. A., & Vonder Haar, T. H. (1995). Observations of the global characteristics and regional radiative effects of marine cloud liquid water. *Journal of Climate*, *8*(12), 2928–2946. https://doi.org/10.1175/1520-0442(1995)008<2928:OOTGCA>2.0.CO;2

Hong, S., & Shin, I. (2013). Wind speed retrieval based on sea surface roughness measurements from spaceborne microwave radiometers. *Journal of Applied Meteorology and Climatology*, *52*(2), 507–516. https://doi.org/10.1175/JAMC-D-11-0209.1

Hood, R. E., Cecil, D. J., LaFontaine, F. J., Blakeslee, R. J., Mach, D. M., Heymsfield, G. M., et al. (2006). Classification of tropical oceanic precipitation using high-altitude aircraft microwave and electric field measurements. *Journal of the Atmospheric Sciences*, *63*(1), 218–233. https://doi.org/10.1175/JAS3606.1

Houze, R. A., McMurdie, L. A., Petersen, W. A., Schwaller, M. R., Baccus, W., Lundquist, J. D., et al. (2017). The olympic Mountains experiment (OLYMPEX). *Bulletin of the American Meteorological Society*, *98*(10), 2167–2188. https://doi.org/10.1175/BAMS-D-16-0182.1

Hwang, P. A., Reul, N., Meissner, T., & Yueh, S. H. (2019). Whitecap and wind stress observations by microwave radiometers: Global coverage and extreme conditions. *Journal of Physical Oceanography*, *49*(9), 2291–2307. https://doi.org/10.1175/JPO-D-19-0061.1

Kummerow, C., Barnes, W., Kozu, T., Shiue, J., & Simpson, J. (1998). The Tropical Rainfall Measuring Mission (TRMM) sensor package. *Journal of Atmospheric and Oceanic Technology*, *15*(3), 809–817. https://doi.org/10.1175/1520-0426(1998)015<0809:TTRMMT>2.0.CO;2

Lang, T., Amiot, C., & Biswas, S. (2021). AMPR CAMP^{2}Ex calibrated & quality-controlled flight dataset level 2B, revision *1*, 16 pp. https://www-air.larc.nasa.gov/cgi-bin/enzFile?c1684C5749C53F525A470B4E964F4D05ABA2f7075622d6169722f5846532f43414d503245582f323031392f5033425f41495243524146542f4c414e472e54494d4f5448592f43414d503245782d414d50525f5033425f323031395f52315f526561645f4d655f46697273742e706466

Liebe, H. J., Hufford, G. A., & Manabe, T. (1991). A model for the complex permittivity of water at frequencies below 1 THz. *International Journal of Infrared and Millimeter Waves*, *12*(7), 659–675. https://doi.org/10.1007/BF01008897

Mathworks. (2025). *Regress: Multiple linear regression*. The Mathworks, Inc. Retrieved from https://www.mathworks.com/help/stats/regress.html. accessed 06 June 2025.

McGrath, A., & Hewison, T. (2001). Measuring the accuracy of MARSS – An airborne microwave radiometer. *Journal of Atmospheric and Oceanic Technology*, *18*(12), 2003–2012. https://doi.org/10.1175/1520-0426(2001)018<2003:MTAOMA>2.0.CO;2

McMurdie, L. A., Heymsfield, G. M., Yorks, J. E., Braun, S. A., Skofronick-Jackson, G., Rauber, R. M., et al. (2022). Chasing snowstorms: The Investigation of Microphysics and Precipitation for Atlantic Coast-Threatening Snowstorms (IMPACTS) campaign. *Bulletin of the American Meteorological Society*, *103*(5), E1243–E1269. https://doi.org/10.1175/BAMS-D-20-0246.1

Miller, D. J., Zhang, Z., Ackerman, A. S., Platnick, S., & Baum, B. A. (2016). The impact of cloud vertical profile on liquid water path retrieval based on the bispectral method: A theoretical study based on large-eddy simulations of shallow marine boundary layer clouds. *Journal of Geophysical Research: Atmospheres*, *121*(8), 4122–4141. https://doi.org/10.1002/2015JD024322

Mülmenstädt, J., Sourdeval, O., Delanoë, J., & Quaas, J. (2015). Frequency and occurrence of rain from liquid-, mixed-, and ice-phase clouds derived from A-Train satellite retrievals. *Geophysical Research Letters*, *15*, 6502–6509. https://doi.org/10.1002/2015GL064604

National Academies of Sciences, Engineering, and Medicine (NASEM). (2018). *Thriving on our changing planet: A decadal strategy for Earth observation from space*. The National Academies Press. https://doi.org/10.17226/24938

National Centers for Environmental Prediction (NCEP). (2000). NCEP FNL operational model global tropospheric analyses, continuing from July 1999 [Dataset]. *National Center for Atmospheric Research, Computational and Information Systems Laboratory*. https://doi.org/10.5065/D6M043C6

O'Dell, C. W., Wentz, F. J., & Bennartz, R. (2008). Cloud liquid water path from satellite-based passive microwave observations: A new climatology over the global oceans. *Journal of Climate*, *21*, 1721–1739. https://doi.org/10.1175/2007JCLI1958.1

Oh, S.-B., Lee, Y. H., Jeong, J.-H., Kim, Y.-H., & Joo, S. (2018). Estimation of the liquid water content and Z–LWC relationship using Ka-band cloud radar and a microwave radiometer. *Meteorological Applications*, *25*(3), 423–434. https://doi.org/10.1002/met.1710

Platnick, S., Meyer, K. G., King, M. D., Wind, G., Amarasinghe, N., Marchant, B., et al. (2017). The MODIS cloud optical and microphysical products: Collection 6 updates and examples from Terra and Aqua. *IEEE Transactions on Geoscience and Remote Sensing*, *55*(1), 502–525. https://doi.org/10.1109/TGRS.2016.2610522

Reid, J. S., Maring, H. B., Narisma, G. T., van den Heever, S., Di Girolamo, L., Ferrare, R., et al. (2023). The coupling between tropical meteorology, aerosol lifecycle, convection, and radiation, during the Cloud, Aerosol and Monsoon Processes Philippines Experiment (CAMP^{2}Ex). *Bulletin of the American Meteorological Society*, *104*(6), E1179–E1205. https://doi.org/10.1175/BAMS-D-21-0285.1

Rosenkranz, P. W. (1993). Absorption of microwaves by atmospheric gases. In M. A. Janssen (Ed.), *Atmospheric remote sensing by microwave radiometry*, *Wiley series in remote sensing and image processing* (Vol. 6, pp. 37–90). John Wiley and Sons. Retrieved from https://dspace.mit.edu/bitstream/handle/1721.1/68611/Absorp_MW_Atmos_Gases.pdf

Rosenkranz, P. W. (1998). Water vapor microwave continuum absorption: A comparison of measurements and models. *Radio Science*, *33*(4), 919–928. https://doi.org/10.1029/98RS01182

Ruf, C., Asharaf, S., Balasubramaniam, R., Gleason, S., Lang, T., McKague, D., et al. (2019). In-orbit performance of the constellation of CYGNSS hurricane satellites. *Bulletin of the American Meteorological Society*, *100*(10), 2009–2023. https://doi.org/10.1175/BAMS-D-18-0337.1

Sinclair, K., van Diedenhoven, B., Cairns, B., Alexandrov, M., Dzambo, A. M., & L'Ecuyer, T. (2021). Inference of precipitation in warm stratiform clouds using remotely sensed observations of the cloud top droplet size distribution. *Geophysical Research Letters*, *48*(10), e2021GL092547. https://doi.org/10.1029/2021GL092547

Sinclair, K., van Diedenhoven, B., Cairns, B., Yorks, J., Wasilewski, A., & McGill, M. (2017). Remote sensing of multiple cloud layer heights using multi-angular measurements. *Atmospheric Measurement Techniques*, *10*(6), 2361–2375. https://doi.org/10.5194/amt-10-2361-2017

Skofronick-Jackson, G., Petersen, W. A., Berg, W., Kidd, C., Stocker, E. F., Kirschbaum, D. B., et al. (2017). The Global Precipitation Measurement (GPM) mission for science and society. *Bulletin of the American Meteorological Society*, *98*(8), 1679–1695. https://doi.org/10.1175/BAMS-D-15-00306.1

Spencer, R. W., Hood, R. E., Lafontaine, F. J., Smith, E. A., Platt, R., Galliano, J., et al. (1994). High-resolution imaging of rain systems with the Advanced Microwave Precipitation Radiometer. *Journal of Atmospheric and Oceanic Technology*, *11*(4), 849–857. https://doi.org/10.1175/1520-0426(1994)011<0849:HRIORS>2.0.CO;2

Tompkins, A. M. (2001). Organization of tropical convection in low vertical wind shears: The role of water vapor. *Journal of the Atmospheric Sciences*, *58*(6), 529–545. https://doi.org/10.1175/1520-0469(2001)058<0529:OOTCIL>2.0.CO;2

Uhlhorn, E. W., Black, P. G., Franklin, J. L., Goodberlet, M., Carswell, J., & Goldstein, A. S. (2007). Hurricane surface wind measurements from an operational stepped frequency microwave radiometer. *Monthly Weather Review*, *135*(9), 3070–3085. https://doi.org/10.1175/MWR3454.1

Vömel, H., Goodstein, M., & Arendt, C. (2020). Dropsonde data quality report: Clouds, Aerosol and Monsoon Processes-Philippines Experiment (CAMP^{2}Ex, 2019). Version 1.0. In *UCAR/NCAR – Earth observing laboratory*. Retrieved from https://www-air.larc.nasa.gov/cgi-bin/ArcView/camp2ex

Wentz, F. J. (1997). A well-calibrated ocean algorithm for special sensor microwave/imager. *Journal of Geophysical Research*, *102*(C4), 8703–8718. https://doi.org/10.1029/96JC01751

Wentz, F. J., & Meissner, T. (2000). Algorithm theoretical basis document (ATBD), version 2: AMSR ocean algorithm. *Remote Sensing Systems Technical Proposal 121599A-1*, 67. https://eospso.gsfc.nasa.gov/sites/default/files/atbd/atbd-amsr-ocean.pdf

Wentz, F. J., & Meissner, T. (2007). Supplement 1: Algorithm theoretical basis document for AMSR-E ocean algorithms. *Remote Sensing Systems Technical Report, 6*, 051707. http://images.remss.com/papers/amsr/AMSR_Ocean_Algorithm_Version_2_Supplement_1.pdf

Wentz, F. J., & Spencer, R. W. (1998). SSM/I rain retrievals within a unified all-weather ocean algorithm. *Journal of the Atmospheric Sciences*, *55*(9), 1613–1627. https://doi.org/10.1175/1520-0469(1998)055<1613:SIRRWA>2.0.CO;2

West, C. G., & Smith, R. B. (2021). Global patterns of offshore wind variability. *Wind Energy*, *24*(12), 1466–1481. https://doi.org/10.1002/we.2641

Wilheit, T. T., & Chang, A. T. C. (1980). An algorithm for retrieval of ocean surface and atmospheric parameters from the observations of the scanning multichannel microwave radiometer. *Radio Science*, *15*(3), 525–544. https://doi.org/10.1029/RS015i003p00525

Wisler, M. M., & Hollinger, J. P. (1977). Estimation of marine environmental parameters using microwave radiometric remote sensing systems. *Naval Research Laboratory Memo. Rep.*, *3661*, 27. https://apps.dtic.mil/sti/html/tr/ADA049507/index.html

Yeh, H.-Y. M., Prasad, N., Mack, R. A., & Adler, R. F. (1990). Aircraft microwave observations and simulations of deep convection from 18 to 183 GHz. Part II: Model results. *Journal of Atmospheric and Oceanic Technology*, *7*(3), 392–410. https://doi.org/10.1175/1520-0426(1990)007<0392:AMOASO>2.0.CO;2

Zhou, J., Lei, H., & Ji, L. (2013). Improvement of liquid water content retrieval accuracy by multilevel detection in cloud tomography. *Journal of Atmospheric and Oceanic Technology*, *30*(2), 301–312. https://doi.org/10.1175/JTECH-D-12-00054.1

Zipser, E. J., & LeMone, M. A. (1980). Cumulonimbus vertical velocity events in GATE. Part II: Synthesis and model core structure. *Journal of the Atmospheric Sciences*, *37*(11), 2458–2469. https://doi.org/10.1175/1520-0469(1980)037<2458:CVVEIG>2.0.CO;2